Experience-dependent modulation of behavioral features in sensory navigation of nematodes and bats revealed by machine learning

Short Title: Machine learning extraction of behavioral features

Authors: Shuhei J. Yamazaki[1], Yosuke Ikejiri[1], Fumie Hiramatsu[1], Kosuke Fujita[1, 5], Yuki Tanimoto[1, 6], Akiko Yamazoe-Umemoto[1],Yasufumi Yamada[2], Koichi Hashimoto[3], Shizuko Hiryu[2], Takuya Maekawa[4], Koutarou D. Kimura[1*]

Affiliations

[1]Department of Biological Sciences, Graduate School of Science, Osaka University, Toyonaka, Osaka 560-0043, Japan

[2]Faculty of Life and Medical Sciences, Doshisha University, Kyotanabe, Kyoto 6100321, Japan

[3]Graduate School of Information Sciences, Tohoku University, Sendai, Miyagi 980-8579, Japan

[4]Department of Multimedia Engineering, Graduate School of Information Science and Technology, Osaka University, Suita, Osaka 565-0871, Japan

[5]Present address: Department of Ophthalmology, Graduate School of Medicine, Tohoku University, Sendai, Miyagi 980-8574, Japan

[6]Present address: RIKEN Brain Science Institute, Wako, Saitama 351-0198, Japan

*Correspondence: kokimura-lab@umin.ac.jp or kokimura@bio.sci.osaka-u.ac.jp

Classification: Biological Sciences, Neuroscience

ABSTRACT

Animal behavior is the integrated output of multiple brain functions. However, understanding how multiple brain functions affect behavior has been difficult. In order to decipher dynamic brain functions from time-series of behavioral data, we developed a machine learning strategy that extracts distinguishing behavioral features of sensory navigation. We first investigated experience-dependent enhancement of odor avoidance behavior of the nematode *Caenorhabditis elegans*. We segmented worms' trajectories during olfactory navigation into two behavioral states, analyzed 92 features of the states, and automatically extracted 9 distinguishing features modulated by prior odor experience using a statistical index, the gain ratio. The extracted features included ones previously unidentified, one of which indicated that the prior odor experience lowers worms' behavioral responses to a small increase in odor concentration, causing enhanced odor avoidance. In fact, calcium imaging analysis revealed that the response of ASH nociceptive neurons to a small odor increase was significantly reduced after prior odor experience. In addition, based on extracted features, multiple mutant strains were categorized into several groups that are related to physiological functions of the mutated genes, suggesting a possible estimation of unknown gene function by behavioral features. Furthermore, we also extracted behavioral features modulated by experience in acoustic navigation of bats. Thus, our results demonstrate that, regardless of animal species, sensory modality, and spatio-temporal scale, behavioral features during navigation can be extracted by machine learning analysis, which may lead to the understanding of information processing in the brain.

SIGNIFICANCE STATEMENT

Behavior is the most important output of brain activity, and its recording has become easy because of the development of small and inexpensive cameras and small GPS devices. However, these "behavioral big data" have been used to calculate very simple indices, such as speed, direction, and goal arrival rate. In this study, we analyzed animal behavior using machine learning (also known as "artificial intelligence") and found specific behavioral features related to navigation in worms and bats. We also found activity changes in nerve cells that were reflected in the worm's behavioral changes. Thus, our results demonstrate that artificial intelligence can be used to find characteristics of animal behavior that would eventually help us understand how the brain works.

Keywords: Navigation, Machine Learning, Behavior

INTRODUCTION

Brain activity can be measured as time series vector data of a large number of neural activities using simultaneous optical monitoring recently (1, 2). Behavior, the integrated output of multiple brain functions such as sensory perception, memory, emotion, and decision-making, however, is still analyzed in classic ways and insufficiently studied using simple and subjectively chosen measures, such as velocity, migratory distance, and/or the probability of reaching to a particular goal. This large asymmetry in data between neural activity and behavior has emerged as one of the significant issues in modern neuroscience (3-5). In other words, without describing when and how behavior changes in detail, we may not be able to fully interpret the meaning of large-scale records of neural activities. One cause for this problem is the difficulty in the analysis of behavior: Although machine-vision techniques over small areas and GPS-based tracking over large areas allow us to continuously monitor the positions and/or postures of animals, it is still unclear which aspects of behavioral features should be focused to clarify the relationships with neural activities.

One way to solve this problem is to use machine learning. Machine learning is a method of extracting latent patterns and discovering knowledge from a large amount of data (6). Machine learning-based behavioral analyses of model invertebrates, such as the fruit fly *Drosophila melanogaster* and the nematode *Caenorhabditis elegans*, have been performed because these model animals are suitable for machine vision monitoring of their behavior due to their small size and relatively simple behavioral patterns (7-13). Furthermore, these animals have relatively small neural circuits, and multiple genetic

techniques are available, suggesting that comprehensive analysis of brain function at behavioral, neuronal, and molecular levels is feasible. These analyses have provided new insights into behavioral states and behavioral motifs during voluntary movement, as well as the relationships between optogenetic activation of neurons and behavioral responses. However, machine learning has not been used to understand the brain activity related to sensory behaviors: How is environmental information transformed into behavioral responses through sensory perception and decision-making, as well as its modulation by memory and/or emotion in the nervous system? The lack of research in this topic is likely due to the fact that these invertebrate model animals are too small to accurately and easily measure sensory input during behavior. In addition, even when sensory input can be measured, the method to effectively reveal the dynamic relationships between sensory input and behavioral output has not been established.

In the present study, we aimed to establish a method to objectively and comprehensively extract behavioral features that are possibly linked to the neural activities for sensory behavior. For that purpose, we analyzed two types of sensory navigation that have been monitored quantitatively but are different in modality and spatio-temporal scale—olfactory navigation of *C. elegans* and acoustic navigation of the bat *Rhinolophus ferrumequinum nippon*—using machine learning. In particular, we focused on experience-dependent modulation (i.e., "learning"; to avoid confusion with machine learning analysis, we do not use this term for biological learning hereafter) of navigation as a model for efficient extraction of differences in behavioral features. In *C. elegans*, experience-dependent behavioral modulation has been studied in thermotaxis

and salt-taxis, in which worms move in a preferred direction by changing the frequency of directional changes depending on the intensity of the sensory stimulus (14). Consistently, changes in neural activity to a stepwise stimulus change have been revealed by calcium imaging mostly of immobilized worms and in a few cases of freely moving worms (15-20). However, it has not been fully clarified how those behaviors are regulated by neural activity that responds to slight changes in stimuli during navigation in a sensory gradient as well as how the behavioral and neural responses are modulated by experience. Furthermore, although large scale analyses of mutant strains are available (12, 21), methods for effectively analyzing the differences in experience-dependent modulation of sensory behaviors of mutant strains have not been established.

To reveal experience-dependent modulations of olfactory navigation in worms, we extracted prominent features of behavior and their relationships to odor stimuli using machine learning. For this, we segmented the animals' navigation into two behavioral states and, for individual states, calculated the gain ratio, a statistical index used in decision tree analysis to identify features that distinguish the data in different classes (22). We chose this method because it allows us to easily interpret the results of the analysis for the planning of physiological experiment of neural activities. In the present study, we analyzed 92 features of behavior and sensory information from each of ~200 behavioral states of wild-type worms either with or without a prior odor experience (25 worms per condition) and found that 9 features are modulated in an experience-dependent manner. One of the extracted features, the reduction in behavioral

response to a small increase in odor concentration, was consistent with a change in neuronal activity revealed by calcium imaging. In addition, we calculated gain ratios to identify the experience-dependent changes in olfactory navigation of multiple mutant strains and found that the mutants were categorized into several groups based on behavioral features, which reflect physiological functions of the mutated genes. Furthermore, we also identified experience-dependent modulation of behavioral features from bat acoustic navigation. Thus, we propose that machine learning analysis with gain ratios is an efficient strategy to reveal features of animal behavior in general.

METHODS

Cultivation of worms

The techniques used for culturing and handling *C. elegans* strains have been essentially described previously (23). Wild type Bristol strain RRID:WB-STRAIN:N2_Male and mutant strains RRID:WB-STRAIN:MT1219 *egl-3(n589)*, RRID:WB-STRAIN:VC671 *egl-3(ok979)*, RRID:WB-STRAIN:CX4544 *ocr-2(ak47),* RRID:WB-STRAIN:JC1636 *osm-9(ky10)*, RRID:WB-STRAIN:JC0570 *tax-4(p678)* were obtained from the Caenorhabditis Genetics Center (University of Minnesota, USA).
RRID:WB-STRAIN:KDK1 dop-3*(tm1356)* was originally obtained from National BioResource Project (Japan) and backcrossed five times with N2 .

Analysis of worms' olfactory navigation

A 2-nonanone avoidance assay was performed as described previously (24, 25). Briefly, 2-3 young adult hermaphrodite worms grown synchronously were placed in the center

of a 9-cm nematode growth media (NGM) plate, and 2 μL of 30% 2-nonanone (cat. no. 132-04173; Wako, Japan) diluted in EtOH (cat. no. 0057-00456; Wako, Japan) were dropped in two spots on the surface of the NGM plate (Fig. 1A top), and the worms' behavior was recorded for 12 min. This assay was performed under the following three conditions: the worms cultivated on NGM plates with their food bacteria RRID:WB-STRAIN:OP-50 were briefly washed with NGM buffer and subjected to the assay ("naive" condition), or they were subjected to the assay after 1 h of preexposure to 0.6 μL of 15% 2-nonanone diluted in EtOH or to only EtOH spotted on the lid of a NGM plate without food ("preexp" and "mock" conditions, respectively). We added the mock-treated control to confirm that 1-h starvation did not affect the odor avoidance behavior of worms and to extract behavioral features modulated by the odor preexposure compared to the naive and the mock-treated controls. Images of worms the NGM plate during odor avoidance assay were acquired by a high-resolution USB camera (DMK 72AUC02; The Imaging Source, USA) with a lens (LM16JC5MW; Kowa, Japan) at 1 Hz for 12 min. From the recorded images, the coordinates of individual animals' centroids were acquired using Move-tr/2D software (Library Co., Ltd., Tokyo, Japan) and used for the following analysis.

Similar to worms' other sensory behaviors, trajectories in the 2-nonanone avoidance assay can be divided into two states: "run", a relatively long period of straight movement, and "pirouette", a period of short movements interrupted by frequent reversals and turns (24, 26). Angular change per s was calculated from the centroid coordinates, and movements of 1 s with angular change larger than 90° were classified

as a turn. A histogram of turn intervals was fitted by two exponentials, suggesting that turn intervals are regulated by two probabilistic mechanisms (25, 26). The time of the intersection of the two exponentials was defined as t_{crit}, and turn intervals longer or shorter than the t_{crit} were classified as runs or included in pirouettes, respectively. t_{crit} was calculated for the control (i.e., naive plus mock-treated) condition for wild-type and mutant strains, respectively. In this study, we analyzed features of runs but not of pirouettes except for their duration because pirouettes appear to have little effect on odor avoidance (25). Excel 2010 (Microsoft Corp.) was used for these calculations. The odor concentrations that worms experienced at specific spatio-temporal points were calculated according to the dynamic odor gradient model based on the measured odor concentration (19).

Bats

As previously described, three adult Japanese horseshoe bats (*Rhinolophus ferrumequinum nippon*, body length: 6.0–8.0 cm, body mass: 20–30 g) were captured from natural caves in Hyogo and Osaka prefectures in Japan (27). The bats were housed in a temperature- and humidity-controlled colony room [4 (L) × 3 (W) × 2 m (H)] with a 12-h-on/12-h-off light cycle at Doshisha University in Kyoto, Japan. The bats were allowed to fly freely and given access to mealworms and water. Captures were conducted under license and in compliance with current Japanese law. All experiments complied with the Principles of Animal Care, publication no. 86-23, revised 1985, of the National Institutes of Health, and with current Japanese law. All experiments were approved by the Animal Experiment Committee of Doshisha University.

200

201 **Bat acoustic navigation**

202 Methods for acoustic navigation measurement in bats have been described elsewhere
203 (Yamada et al., in revision). In brief, the experiments were conducted in a flight
204 chamber, which was constructed of steel plates [9 (L) × 4.5 (W) × 2.5 m (H)] under
205 lighting with red filters (>650 nm) to avoid visual effects on the bats. An obstacle
206 environment was constructed using plastic chains (4 cm in diameter) that were
207 suspended from the ceiling of the chamber. The chains were arranged at 15-cm intervals
208 in the *x*-axis and at 22-cm intervals in the *y*-axis so that the bat was forced to fly in an
209 S-shaped pattern without passing between chains. With this layout, three naive bats
210 were used: each bat was observed for 12 continuous repeated flights so that
211 echolocation behaviors in unfamiliar and familiar spaces could be compared. In this
212 study, the initial three flights were defined as unfamiliar flights, and the last three flights
213 were defined as familiar flights.

214

215 The flight behavior of the bats was recorded using two digital high-speed video cameras
216 (MotionPro X3; IDT Japan, Inc., Japan) at 125 frames/s, which were located in the left
217 and right corners of the flight chamber. Based on a direct linear transformation
218 technique, the successive 3D positions of the flying bats, as well as the locations of
219 other objects, were reconstructed using motion analysis software (DIPPMotionPro
220 ver. 2.2.1.0; Ditect Corp., Japan). The flight velocity vector of the bat was calculated as
221 the time derivative of the coordinates of its flight trajectory.

222

Behavioral parameters included in a feature vector

For the machine learning analysis of worm olfactory navigation, the following behavioral features were calculated for each run from the centroid coordinates of the worms: start time (*RunTime*), serial number (*RunNum*), velocity (*V*), bearing (*B*), odor concentration that a worm experienced during run (*C*), directionality ratio (*Dir*) (28), run's curvature (called weathervane; *WV*) (29), run duration (*RunDur*), and duration of pirouette just before the run (*PirDur*). Time-differential values were calculated for *V* (*dV*), *B* (*dV*), and *C* (*dC*). For these values, the average (*Ave*) during a run as well as average values over 2 s at the initiation (*Ini*) and at the termination (*Ter*) of a run were also calculated. For *Ini* and *Ter*, 0-2 s after the initiation and 2-4 s before the termination of a run were used; we did not use 0-2 seconds before the termination because previous studies revealed that a worm's speed drops largely during this period (25, 26). Although the time windows for worms were set based on the previous studies, the optimal time windows for bats were calculated by machine learning (see below). In addition, to analyze whether these features are independent for each run (in other words, whether any long-term trend among runs across a pirouette exists), we also calculated hysteretic effects (Δ) of these run features between successive runs for *V*, *dV*, *B*, *dB*, *C*, and *dC*—in fact, a certain relationship between bearings before and after a pirouette (*B_Ini*Δ*Ter*) has been reported in salt-taxis (26). For this, *Ave*, *Ini,* or *Ter* of each run feature was subtracted from any of the previous run features. Hysteretic effects were calculated for just one feature for *RunDur*, *PirDur*, and *WV*, which only possess one value per run, and not calculated for *RunTime* and *RunNum*. A total of 92 features were calculated by combining all these features.

For analysis of changes in the flight of the bats, the following behavioral features in each flight were calculated from the coordinates of the animals and obstacles: three-dimensional flight velocity (*V*), horizontal and vertical bearings of the flight (*B_hori* and *B_vert*, respectively), distance (*R_obs*) and bearing (*B_obs*) of the bat to the nearest edge point of the obstacle chain array, longitudinal directional distance to the frontal chain array (*R_x*), lateral directional distance to the inside pitch of the chain array (*R_y*). Time-differential values were calculated for *V* (*dV*), *B* (*dB*), *dB* (*ddB*), and the flight height (*dH*), which were calculated with frame units of the high-speed video cameras (1/125 s). All flight trajectories were divided into three segments: earlier, middle, and later terms. The time window for the analysis of each behavioral feature was 0.1, 0.2, or 0.3 s before or when ($t = 0$) passing through the chain array. A total of 42 features were calculated by combining all these features.

Excel 2010 and Visual C# (Microsoft) were used for the calculations, and the Beeswarm package for R software (The R Project) was used for the scattered plot of data. These parameters are listed in Table 1 for worms and in Table 4 for bats.

Behavioral classification with gain ratio

In order to extract useful features, we calculated the gain ratio used in C4.5 decision tree analysis (30) for each feature. In decision tree analysis, the amount of information, which is acquired when a group of data is divided into sub-groups by a certain feature, is calculated as information gain. In other words, when dividing a group into sub-groups

by applying a certain feature, information gain is an index indicating the amount of the increased bias of data in the sub-groups after the division. The information gain was then divided by split info, a degree of division, for normalization to compute the gain ratio. For worm olfactory navigation, we extracted behavioral features that have positive gain ratios in naive versus preexposed worms or in mock-treated versus preexposed worms. Then, we chose the features that were common in both comparisons as "features modulated in experience-dependent manner". For bat acoustic navigation, behavioral features were extracted from the comparison of unfamiliar flights (1^{st}-3^{rd}) and familiar (10^{th}-12^{th}) flights. Weka software (the University of Waikato, New Zealand) (31) was used for the calculation.

Calcium imaging

Calcium imaging of the worms' ASH neurons was performed according to a previous report (19). Briefly, transgenic strains expressing GCaMP3 (32) and mCherry (33) in ASH sensory neurons under the *sra-6* promoter (KDK70034 and KDK70072; 20 ng/µl of *sra-6p::GCaMP3*, 20 ng/µl of *sra-6p::mCherry*, 10 ng/µl of *lin-44p::GFP*, 50 ng/µl of PvuII-cut N2 genomic DNA as a carrier in N2 background) were placed on an NGM agar plate on a robotic microscope system, OSB2 (19). Although these transgenic worms were immobilized with the acetyl choline receptor agonist levamisole (34) for high-throughput data acquisition by simultaneous imaging of multiple worms, the previous study revealed that the ASH activity is essentially unaffected by levamisole-treatment (19). For these worms, a constant gas flow of 8 mL/min was delivered, in which the mixture rate of 2-nonanone gas versus the air was changed to

make a temporal gradient of the odor concentration. The temporal change in odor concentration was measured by a custom-made semiconductor sensor before and after the series of calcium imagings on each day. The fluorescence signals of GCaMP3 and mCherry in ASH neurons were divided into two channels using W-View (Hamamatsu, Japan), an image splitting optic, and captured by an EM-CCD camera (ImagEM; Hamamatsu, Japan) at 1 Hz. The intensities of fluorescence signals from cell bodies were extracted and quantified by ImageJ (NIH) after background subtraction. The average ratio over 30 s prior to the odor increase was used as a baseline (F_0), and the difference from F_0 (ΔF) was used to calculate the fluorescence intensities of GCaMP3 and mCherry ($F = \Delta F/F_0$). The ratio between florescence intensities of GCaMP and mCherry (GCaMP/mCherry) was used in the figure.

Statistical analysis

For comparisons of behavioral features among naive, mock-treated, and preexposed worms, the Kruskal-Wallis multiple comparison test followed by the *post hoc* Dunn's test were used (Fig. 2, 3 and 4), except for in the analysis of directional data, for which the Mardia-Watson-Wheeler test was used. The calculations were performed with Prism ver. 5.0 for Mac OSX (GraphPad Software, CA, USA), R (The R Project) or SPSS version 23 (IBM Corp.).

RESULTS

A strategy for extracting features of sensory navigation that were modulated by prior experience

315 In this study, we aimed to extract behavioral features using machine learning to
316 understand changes in information processing in the brain during sensory navigation.
317 However, identifying characteristic changes in behavior and sensory stimulus during
318 navigation has been difficult. It is because sensory stimulus in general changes
319 gradually and continuously during navigation, which may cause gradual or sudden
320 response at some aspects of behavior with certain probabilities. In order to efficiently
321 extract behavioral features of sensory navigation by machine learning, we considered
322 the following points for the analysis: (1) segmenting behavioral states, (2) representing
323 the animal's position as a single point, (3) calculating sensory information, and (4) using
324 a statistical index, gain ratio.
325
326 ***Segmenting behavioral states***
327 Segmentation is one of the important preprocessing steps of a large dataset for effective
328 analysis (35).We considered an animal's navigation to be a series of transitions among a
329 limited number of behavioral states for a certain period, and we analyzed features in
330 each of the behavioral states instead of analyzing features in an entire navigation
331 trajectory or in very short temporal unit (i.e., second or sub-second). For worm
332 olfactory navigation, we segmented the navigation into two well-established behavioral
333 states: runs and pirouettes (14, 26; see METHODS for details). For bat acoustic
334 navigation, we considered the period from passing one obstacle (or from the starting
335 point) until passing the next obstacle as one behavioral state.
336
337 ***Representing animal's position as a point***

338 During a behavioral state in navigation, animals move a certain distance. For the sake of
339 proper dimensionality reduction, we calculated the trajectories of a point representing
340 animal's position (centroid for worms and head position for bats), instead of the posture
341 of an animal, whose description requires more detailed spatial and temporal
342 information.
343
344 ***Sensory information***
345 Sensory information is a key factor affecting an animal's behavior. However, because
346 of technical difficulties, it has been included in the analysis of sensory navigation only
347 in a few cases for small model animals (17, 19, 36). We included the information of
348 odor concentration, which changes dynamically during navigation of worms, as
349 revealed by the direct measurement of odor concentrations in specific spatio-temporal
350 points in a behavioral arena (19).
351
352 ***Gain ratio***
353 To comprehensively examine behavioral features that can be modulated by prior
354 experience, we focused on a statistical index used in machine learning-based
355 classification analysis. In general, classification analysis is the task of classifying new,
356 unlabeled data into appropriate classes using characteristic features and their parameters
357 that have been extracted from the known class-labeled data. In the present study,
358 however, the classification itself was not meaningful because the data were already
359 classified, such as with or without prior experience or wild-type versus mutant strains.
360 Instead, we focused on the procedure in the classification that finds features useful for

361 distinguishing between the two classes. In other words, behavioral features modulated
362 by prior experience should be able to effectively classify the behavioral data of animals
363 with or without this experience.
364
365 For this purpose, we chose to use gain ratio, the index for decision tree analysis (22).
366 Binary decision tree analysis is performed to split a data set into two sub-groups by
367 automatically selecting the best feature and its parameter that has the largest
368 information gain, the difference of the uncertainty ("information entropy") before and
369 after division; each data point is classified into either of the sub-classes based on
370 whether it has a larger or smaller value than the threshold. When applied for binary
371 classification, decision tree analysis automatically evaluates the classification
372 performance of all of a large number of features that are designed by the researchers.
373 The result of this analysis is the extraction of certain features, which allows us to easily
374 understand the usefulness of particular features for the classification. This is a
375 substantial difference from the analysis by support vector machines and/or deep neural
376 networks, where the relationships between features of the data and the classification are
377 not easily discernible (see DISCUSSION).
378
379 **Behavioral features modulated by the prior experience in worm odor avoidance**
380 **behavior**
381 We analyzed the experience-dependent enhancement of odor-avoidance behavior of *C.*
382 *elegans* as a model. We have reported that preexposure of worms to the repulsive odor
383 2-nonanone causes enhancement of avoidance behavior to the odor. After 1 h of

384 preexposure, worms migrate farther away from the odor source as a type of
385 non-associative middle-term learning (24). A series of genetic analyses indicated that
386 neuropeptide and dopamine signaling pathways are required for acquisition and
387 execution of the odor memory, respectively (25), suggesting that this non-associative
388 middle-term memory is caused by a circuit-level modulation of neural activity rather
389 than simple sensory sensitization.
390
391 Previous studies analyzed several features and revealed that run duration is the major
392 behavioral change caused by odor preexposure, likely because of reduction in the
393 pirouette initiation rate (24, 25). However, this did not rule out the possibility that other
394 behavioral features play more profound effects. Moreover, multiple mutant strains
395 exhibit their own abnormalities in the enhanced odor avoidance behavior (see below),
396 although identification of the features modulated in each mutant strain is
397 time-consuming and laborious. To reveal features modulated by prior experience
398 comprehensively and effectively, we calculated the gain ratio by comparing naive
399 versus preexposed and mock-treated versus preexposed animals, and we considered
400 features that were extracted from both comparisons.
401
402 In the machine learning analysis, we calculated gain ratios of 92 features (Fig. 1 and
403 Table 1; see METHODS for details) and extracted 18 and 15 features from the
404 comparisons of naive versus preexposed and mock-treated versus preexposed worms,
405 respectively (Table 2). Nine features were shared between the two comparisons,
406 suggesting that those features were modulated by the prior experience to cause the

enhanced odor avoidance (Table 2 and Fig. 2A). These features are related to run duration (*RunDur*), temporal differences in bearing (*dB_X*), odor concentration (*C_X*), and its temporal difference during runs (*dC_X*). Modulation of run duration (*RunDur*; Fig. 2B) by the prior odor experience was previously revealed by traditional analysis (24). Thus, this result supports the validity of the machine learning analysis.

Experience-dependent modulations of temporal differences in bearing (*dB_X*; Fig. 2C for example and Table 2) have not been revealed previously. Its contribution to the enhancement of avoidance distance, however, are unclear. Differences between the average or the terminal bearing change and the previous initial value (*dB_Ave*Δ*Ini* or *dB_Ter*Δ*Ini*) were also extracted (Table 2), while the differences were likely due to the modulation in the previous initial value (Δ*Ini*), not due to the change in hysteretic effects.

Odor stimuli during runs, which likely drive the worms' odor avoidance behavior, were also found to be modulated in several aspects: the initial, terminal, and average odor concentration (*C_Ini*, *C_Ter*, and *C_Ave*), and the terminal and average odor concentration change (*dC_Te*r and *dC_Ave*) (Table 2; Fig. 2D and E for *C_Ave* and *dC_Ave*, respectively, for examples). However, this result does not directly imply that the lower odor concentration is the causal reason for the enhanced avoidance distance; one possible scenario is that, because the odor-experienced worms were located farther away from the odor source, they sensed a lower concentration of the odor.

Because the terminal and average values of odor concentration change (*dC_Ter* and *dC_Ave*) were extracted, and because a previous study demonstrated that worm odor avoidance behavior depends on *dC*, rather than *C*, at least in naive conditions (19), we investigated these features more in detail. We compared ensemble averages of *dC/dt* that worms sensed during the last 30 s of each run (Fig. 2F). Interestingly, although most of the control (*i.e.* naive and mock-treated) worms sensed 2-3 μM odor concentrations (Fig. 2D), *dC/dt* at the end of each run was ± 0.1 nM/s on average (Fig. 2F; 0.09 ± 0.72 and -0.09 ± 0.76 nM/s for naive and mock-treated animals, respectively). This result suggests that, to initiate a pirouette, worms respond to a subtle odor concentration change, of which the magnitude is 1/20,000 - 1/30,000 of the odor concentration itself per second. Even considering that sensory information is temporally integrated for a few seconds during worm chemosensory navigation (19, 37), this value is far lower than the general psychological threshold for sensory signals: The lower threshold of signal change (ΔS) is more than 1/100 of the signal intensity (S) (38).

This extreme sensitivity to positive *dC/dt* was modulated by prior experience of the odor. The terminal *dC/dt* was significantly higher than in naive and mock-treated animals (1.58 ± 0.6 nM/s compared to the values in the previous paragraph; $p < 0.01$, the Kruskal-Wallis multiple comparison test followed by the *post hoc* Dunn's test). This change in terminal *dC/dt* could be the cause for the enhanced odor avoidance behavior and suggest the following model: the worms without prior experience of the odor are highly sensitive to a slight increase in odor concentration during a run, which is a sign of inappropriate movement toward the source of the repulsive odor, and they respond to

453 it by initiating a pirouette. In contrast, the worms with prior odor experience ignore the
454 slight odor increase and continue the run, which leads to a longer run duration (Fig.
455 2G).
456
457 **The responsiveness of sensory neurons to odor increases was modulated by odor**
458 **experience**
459 If the change in sensitivity to positive *dC/dt* is the causal reason for the enhanced odor
460 avoidance behavior, it should be associated with changes in neural activity. Thus, we
461 analyzed the responsiveness of a likely candidate group of neurons, ASH nociceptive
462 neurons (39, 40). Previously we established the OSB2 microscope system that allows
463 for calcium imaging of *C. elegans* neurons *in vivo* under odor stimuli resembling ones
464 that worms experience during the odor avoidance assay in the plates (19). Using the
465 OSB2 system, we found that ASH neurons are the major sensory neurons to cause
466 pirouettes upon increases in 2-nonanone concentration (19). However, whether the ASH
467 response is modulated by 2-nonanone experience has not been studied.
468
469 We found that ASH responses were modulated by prior odor experience in a manner
470 consistent with the behavioral modulation. When the worms were stimulated with 5
471 nM/s odor increase, which is the lowest rate of change to cause the threshold-level
472 behavioral response in the previous study (19), ASH neurons in naive as well as
473 mock-treated worms exhibited robust responses (Fig. 3A and B). However, the ASH
474 responses were significantly reduced in the preexposed animals (Fig. 3B and C). This
475 result suggests that prior odor experience causes the reduced response to the odor

476 increase, which causes longer run durations and enhanced odor avoidance behavior.

477

478 **Extracted behavioral features of mutant strains correspond to gene functions**

479 We also investigated whether feature extraction from behavior of mutant strains can
480 allow us to understand relationships between chemosensory behavior and gene
481 functions in the nervous system. By calculating gain ratios, we analyzed mutants of
482 genes that are known to be involved in the experience-dependent modulation of
483 2-nonanone avoidance behavior, such as that for proprotein convertase (required for
484 neuropeptide signaling), EGL-3 (41), and the D2-type dopamine receptor DOP-3 (25,
485 42), as well as genes involved in sensation of chemical signals, such as those for TRP
486 channel homologs OCR-2 and OSM-9 (43, 44) and the cGMP-gated cation channel
487 TAX-4 (45), whose relationships to the 2-nonanone avoidance behavior have not been
488 studied.

489

490 *egl-3*, encoding a homolog of proprotein convertase, is required for neuropeptide
491 biosynthesis, expressed in many neurons, and known to be involved in various aspects
492 of worm behavior including learning (25, 41, 46). Deletion and missense mutations of
493 the gene are known to cause severe and mild phenotypes, respectively (25, 47). Our
494 previous study revealed that run duration is not increased after preexposure in *egl-3*
495 mutants, suggesting that neuropeptide signaling is required for the acquisition of odor
496 preexposure memory (25). In the present study, the abnormal features were similar
497 between deletion (*ok979*) and missense (*n589*) mutants, namely, run duration
498 (*Run_Dur*), odor concentration (*C_Ave*, *C_Ini*, *C_Ter*), and odor concentration change

(*dC_Ave*, *dC_Ter*), although the deletion mutants exhibited additional abnormal features (Table 3 and Fig. 4). Increases in odor concentration in preexposed worms were interesting because they were observed only in *egl-3* mutants but not in any other mutants.

Mutations in *dop-3*, which encodes a homolog of the D2-type dopamine receptor, were previously found to affect migratory direction after preexposure (25). This was concluded because the mutants did not exhibit enhanced avoidance distance, although run duration was increase after preexposure, and because run terminal bearing (*B_Ter*) was worsened (25). These features were extracted in this analysis (Table 3), further supporting the reliability of this analysis. In addition, the averaged directionality ratio (*Dir_Ave*) was worsened (Table 3 and Fig. 4C). This is also consistent with the idea that migratory direction is worsened in *dop-3* mutants after preexposure. Moreover, lowered velocity (*V_Ave*, *V_Ter*; Table 3 and Fig. 4B) was also extracted, which may also contribute to the failure in the enhanced odor avoidance. Such multiple abnormal phenotypes are consistent with the fact that *dop-3* is expressed in many neurons and involved in the regulation of multiple aspects of behavior (48).

ocr-2 and *osm-9* both encode homologs of TRP-type cation channels, expressed in multiple sensory neurons including ASH neurons and considered to be involved in sensory perception as well as its modulation (43). We found that mutants for these two genes did not exhibit significantly enhanced odor avoidance (Fig. 4A). In addition, these mutants exhibited increases in velocity (*V_Ave* and *V_Ter*) after preexposure,

522 which was specific for these two mutants but not observed in other mutants. Some
523 features are specific for each mutant strains, which may reflect the differences in their
524 expression and/or function (43). Mutants of *tax-4*, encoding a homolog of the
525 cGMP-gated cation channel expressed in different sets of sensory neurons, exhibited a
526 unique pattern of features (Table 3, Fig. 4).
527
528 Taken together, our results suggest that the pattern of extracted features from mutant
529 strains may reflect functional groupings of the mutated genes. Thus, profiling and
530 classification of extracted mutant features of unknown genes may be useful to estimate
531 their physiological functions.
532
533 **Feature extraction of experience-dependent modulation of acoustic navigation of**
534 **bats**
535 To demonstrate the general applicability of our method, we examined features of
536 acoustic navigation in bats. We have previously reported that bats improve their flight
537 trajectory in an indoor space with obstacles in an experience-dependent manner
538 (Yamada et al., in revision). Here, we analyzed 42 features using gain ratios and
539 extracted several features, such as velocity (*V*), distance to the obstacle chain array
540 (*R_obs* and *R_x*), and horizontal bearing of the flight (*B_hori*) (Table 4 and Fig. 5A-C).
541 Interestingly, although velocity (*V*) itself was modulated by flight experience,
542 acceleration (*dV*) was not (Fig. 5D), suggesting that bats may determine flight speed
543 before initiating but not during navigation, at least in our experimental conditions.
544 Because the bats' vocalizations reflect their attention or decisions (49), our results

545 suggest that such higher brain functions during navigation could be extracted by
546 machine learning analysis.
547
548 **DISCUSSION**
549 In the present study, we extracted behavioral features that are modulated by experience
550 from olfactory navigation of worms and from acoustic navigation of bats using machine
551 learning analysis. In the case of worm olfactory navigation, we found a neural correlate
552 for one of the newly identified features: The reduced behavioral response to an increase
553 in odor concentration was consistent with the reduced response of ASH nociceptive
554 neurons to a small increase in odor concentration. In addition, we also found that mutant
555 strains can be grouped based on extracted features, which may correspond to the
556 physiological roles of genes in chemotaxis and/or experience-dependent modulation.
557 Furthermore, our machine learning analysis was applied to acoustic navigation of bats
558 to extract the features modulated by prior experience.
559
560 **Extraction of behavioral features by machine learning**
561 Machine learning has been playing a major role in classifying behavioral data of model
562 animals into several categories (7-13, 50). Instead of such behavioral classification,
563 however, we intended to use a machine learning technique for extracting characteristic
564 features of sensory behavior to decipher information processing in the brain. For that
565 purpose, we first hypothesized that a change in a behavioral feature reflects a change in
566 activity of a functional unit of the brain. Then, we used machine learning to extract
567 behavioral features that differ between two classes of behavior, rather than to categorize

568 the behavioral data into two classes; in our study, two classes (e.g., "with or without
569 prior experience" or "wild-type versus mutant strains") were determined *per se* and did
570 not need to be categorized.
571
572 In addition, we also included sensory information that worms experienced during the
573 course of behavior in the machine learning analysis. Although small model animals
574 such as *C. elegans* or *Drosophila melanogaster* are suitable for machine vision
575 monitoring and subsequent quantitative analysis of behavior, their small size makes it
576 difficult to measure sensory signals they receive during behavior. We have solved this
577 problem by precisely measuring the odor concentration at multiple spatio-temporal
578 points in a paradigm to assess olfactory behavior of worms (19), which allowed us to
579 include the information of odor concentration and its temporal changes (*C* and *dC*) into
580 the feature vector for the machine learning analysis. Our machine learning method
581 could also be used for detailed analysis of sensory navigation in the environment where
582 the gradients of chemical signal were also quantitatively monitored (36, 51, 52).
583
584 As a result, we were able to find multiple behavioral features modulated by prior
585 experience, including the temporal odor concentration change (*dC_Ter*), which was
586 consistent with the experience-dependent change in the responsiveness of ASH
587 nociceptive neurons. Such an effective and objective approach to estimate neural
588 function from comprehensive behavioral analysis may play important roles in the
589 understanding of recent large-scale monitoring of neuronal activity (see below).
590

For machine learning-based classification, support vector machines and deep learning have also been used (53, 54). However, in these analyses, it is difficult for researchers to understand which features are characteristic to each group because these algorithms attempt to combine multiple features in a single representation. In other words, it is difficult to use the results of classification for subsequent experiments and/or analysis to further investigate the neural correlates of the behavioral differences. In contrast, in the calculation of gain ratio, all features are evaluated independently, allowing us to immediately translate the results of analysis to a new understanding and/or hypothesis for subsequent experiments and analyses, as shown in the present study. Thus, we conclude that the method used in this study—making a list of characteristic features based on gain ratios and subsequently performing detailed analyses on each of extracted features—is effective to understand the basic principles of neural functions regulating behavior.

However, causal relationships among extracted features should be considered carefully. For example, because odor concentration (C) and temporal odor concentration change (dC) are both features of sensory stimuli, they were likely candidates for the cause of changes in behavioral response. However, we regard that dC, rather than C itself, is the causal reason because of the following: (1) previous quantitative analysis in the plate assay paradigm revealed that pirouettes and runs are strongly correlated with positive or negative dC, respectively, rather than the value of C; (2) in the OSB2 robotic microscope system, positive or negative dC caused high or low levels of turning, such as pirouettes and runs, respectively (19). For example, the lower C in preexposed

worms is likely caused by their relatively lower positions in the odor gradient (i.e., farther positions from the odor source) caused by the enhanced avoidance behavior. In other words, sensory behaviors are closed loops—changes in sensory input cause changes in behavior, while changes in behavior should also cause changes in sensory input because the positions and/or directions of sensory organs are changed due to the behavior. Thus, even when sensory features are extracted by machine learning, causal relationships with behavioral features should be evaluated by independent experiments: An open loop system, which allows control of sensory stimuli and monitoring behavior independently, such as the OSB2 system (19), will provide an effective solution.

Analysis of multiple mutant strains revealed that the extracted features appeared to be correlated with the physiological roles of the genes. For example, two alleles of a gene required for neuropeptide signaling (*egl-3*) exhibited similar feature patterns, which were different from mutants of a dopamine-signaling gene (*dop-3*). In addition, mutations in two homologous but distinct TRP-type channel genes required for sensory signaling (*ocr-2* and *osm-9*) exhibited a similar feature pattern, and the one for cyclic nucleotide-gated ion channels (*tax-4*) exhibited a different pattern. It is interesting that mutants of genes with similar functions exhibited similar behavioral features although these genes should influence animal behavior in a complex manner. These results suggest that behavioral features of mutants of a novel gene may be categorized to a group of genes which have similar physiological functions. In other words, feature extraction using gain ratio of multiple mutant strains can allow estimation of gene functions in the nervous system.

637

638 In conclusion, we established a machine learning method to effectively reveal different
639 features of two different sensory behaviors. In particular, it is important to include not
640 only the behavior itself but also environmental sensory information that animals sense
641 in the feature vectors. Furthermore, it is also necessary to verify causal relationships of
642 the extracted features by other methods, such as using an open loop experimental setup.
643 In addition, this method can be used for estimation of the physiological function of
644 genes.

645

646 This method could be applied to analysis of more complex behaviors of other animals.
647 In the case of visual and acoustic stimuli, it is not clear what features of the stimuli (e.g.,
648 shapes, colors, and brightness for visual stimuli, and frequency and intensity for
649 acoustic stimuli) have the most prominent effects on behavior in a particular context.
650 We believe that our method presented herein, which allows extraction of the essential
651 features of information processing for sensory behaviors in the brain in an objective and
652 comprehensive manner, will help to solve this problem. Poor description of behavior
653 with simple indices compared to "big data" on neuronal activity is being recognized as
654 one of the significant problems in modern neuroscience (3-5). We expect that
655 comprehensive and objective feature extraction would increase the wealth of description
656 of behavior, which will provide us clues to understand more of the big data from brain
657 activity monitoring.

658

659 **FIGURE LEGENDS**

Figure 1. A workflow of the machine learning method for the analysis of worm odor avoidance behavior; "Behavioral data" (Top) Examples of the trajectories of 3 worms during 12 min of 2-nonanone avoidance assay, overlaid on a schematic drawing of a 9-cm agar plate. (Second from the top) A magnified view of trajectories of a worm, in which runs are blue and pirouettes are red. (Second from the bottom and bottom) Graphs showing the odor concentration (*C*, second from the bottom) and temporal changes in *C* (*dC*, bottom) at the worm's position at 1-s intervals during the odor avoidance assay. "Feature vector" From the (*x*, *y*) coordinates of each worm's centroid, velocity, bearing, odor concentration, and their derivatives (*V*, *B*, *C*, *dV*, *dB*, and *dC*) as well as the difference between the present and the previous values (Δ) were calculated. "Gain ratio" One example (*C_Ter*) of calculating gain ratio is shown.

Figure 2. Extracted features that were modulated by prior experience of the odor. (A) Enhanced odor avoidance behavior of worms caused by odor preexposure. (Left) End points of 25 worms in each condition plotted on a schematic drawing of the assay plate. (Right) Avoidance distance (distance between the center line of the plate and end point of behavior) of each worm. Each bar represents median. Significant differences were observed in the preexposed worms compared to the naive and mock-treated worms (***$p < 0.001$, Kruskal-Wallis test with *post hoc* Dunn's test). (B, C, D and E) Distributions of extracted features. Duration (B), the initial value of bearing change (C), the average odor concentration (D), and the average odor concentration change (E) of each run (**$p < 0.01$ and ***$p < 0.001$, Kruskal-Wallis test with *post hoc* Dunn's test). t_{crit} for wild type worms was 13.1. Bars represent median and first and third quartiles.

683 (F) Time course changes in ensemble averages of odor concentration (*dC*) that worms
684 experienced before the termination of runs. On average, naive and mock-treated worms
685 experienced odor decrements of about -8 nM/s until 15 s before the end of each run,
686 when the decrements started to become very close to zero at the end of the run. In
687 contrast, preexposed animals consistently experienced smaller (i.e., shallower) odor
688 decrements during runs, and the average odor concentration changes at the end of runs
689 were positive. Bars represent mean ± SEM. (G) A model relationship between odor
690 concentration change and behavioral response during navigation along the odor gradient.
691 When naive and mock-treated worms sensed a slight increase in the odor concentration,
692 which is a sign of migrating in the wrong direction, they stopped a run and started a
693 pirouette to search for a new direction. In contrast, the preexposed worms did not
694 respond to a slight increase in odor concentration, leading to longer run durations and
695 shorter pirouette durations in total, which likely contribute to the enhanced avoidance
696 distance. Numbers of worms are 25 for all the conditions, and all the statistical details
697 are described in Supplementary Table 1.
698
699 Figure 3. Sensory responses to slight odor concentration increases were reduced by
700 preexposure to the odor. (A) A schematic drawing of calcium imaging of neural activity
701 of worms under odor stimuli. Several immobilized worms were simultaneously exposed
702 to an odor flow whose concentration was changed by controlling syringe pumps. (B)
703 Responses (GCaMP/mCherry) of ASH neurons in naive (n = 25), mock-treated (n = 29),
704 and preexposed (n = 26) worms. Thick colored lines with gray shadows indicate mean ±
705 SEM, and thin lines indicate individual responses. (C) Distributions of peak values

706 during the odor-increasing phase (t = 40-80 s) shown in panel B. Bars represent median.
707 (***$p < 0.001$, Kruskal-Wallis test with *post hoc* Dunn's test).
708
709 Figure 4. Examples of extracted features of mutant strains. Avoidance distance (A), the
710 average velocity (B), the average migratory direction (C), and the initial odor
711 concentration (D) per run are shown. t_{crit} for each strain was 8.1 (*egl-3(n589)*), 7.2
712 (*egl-3(ok979)*), 18.1 (*dop-3(tm1356)*), 11.2 (*ocr-2(ak47)*), 17.8 (*osm-9(ky10)*), and 6.7
713 (*tax-4(p678)*). Thick bars represent statistical differences between preexposed worms
714 versus naive *and* mock-treated worms, suggesting differences caused by the odor
715 preexposure; thin bars represent statistical differences between preexposed worms
716 versus naive *or* mock-treated worms, which were not caused by the preexposure. (**$p <$
717 0.01 and ***$p < 0.001$, Kruskal-Wallis test with *post hoc* Dunn's test)
718
719 Figure 5. Experience-dependent changes in bat acoustic navigation. (A) Measurement
720 system for 3D flight trajectory of a bat during obstacle avoidance flight in a chamber.
721 (B) Representative flight trajectories of a bat in horizontal plane during repeated flight
722 in the obstacle course. The top figure combines the initial three (red) and last three
723 (blue) flight trajectories. Each behavioral feature was collected in three segments:
724 earlier, middle, and later terms. Bottom figure shows an expanded view of the earlier
725 term in the first flight. Definition of the horizontal bearing of the flight (*B_hori*),
726 distance (*R_obs*), and bearing (*B_obs*) of the bat to the nearest edge point of the
727 obstacle chain array, longitudinal directional distance to the frontal chain array (*R_x*),
728 and lateral directional distance to the inside pitch of the chains array (*R_y*) are indicated.

729 Time windows for the analysis of each behavioral feature were 0.1, 0.2, or 0.3 s before
730 or when ($t = 0$) passing through the chain array. (C) A list of extracted features of bat
731 acoustic navigation modulated by flight experience. (D) Distributions of *V(-0.3)* and
732 *dV(-0.3)* are plotted. Bars represent median and first and third quartiles. (*$p < 0.05$,
733 Kruskal-Wallis test with *post hoc* Dunn's test).
734
735
736 **ACKNOWLEDGEMENTS**
737 We thank Drs. André Brown, Katsuyoshi Matsushita, Ken-ichi Hironaka, Takuma
738 Degawa, and the Kimura laboratory members for suggestions and comments on this
739 work. Nematode strains were provided by the Caenorhabditis Genetics Center (funded
740 by the NIH Office of Research Infrastructure Programs P40 OD010440) and by
741 National Bioresource Project funded by the Ministry of Education, Culture, Sports,
742 Science and Technology (MEXT), Japan. This work was supported by Interdisciplinary
743 graduate school program for systematic understanding of health and disease (for S.J.Y.),
744 by KAKENHI 25249020 and JP16H06536 (for K.H.), JP16H06542 (for S.H.),
745 JP16H06539 (for T.M.), JP16H06545 (for K.D.K.) from the MEXT, by PRESTO
746 JPMJPR14D8 (for S.H.) by JST, and by Osaka University Co-Creation Program (for
747 T.M. and K.D.K.).
748
749 **AUTHOR CONTRIBUTIONS**

S.J.Y, T.M. and K.D.K. designed the experiments, S.J.Y, Y.I., F.H., K.F., Y.T., Y.Y., K.H., S.H. and K.D.K. performed the experiments, S.J.Y. and T.M. analyzed the data, and S.J.Y. and K.D.K. wrote the manuscript. All authors reviewed the manuscript.

REFERENCES

1. Alivisatos AP, et al. (2012) The Brain Activity Map Project and the Challenge of Functional Connectomics. *Neuron* 74(6):970–974.

2. Landhuis E (2017) Neuroscience: Big brain, big data. *Nature* 541(7638):559–561.

3. Krakauer JW, Ghazanfar AA, Gomez-Marin A, MacIver MA, Poeppel D (2017) Neuroscience Needs Behavior: Correcting a Reductionist Bias. *Neuron* 93(3):480–490.

4. Gomez-Marin A, Paton JJ, Kampff AR, Costa RM, Mainen ZF (2014) Big behavioral data: psychology, ethology and the foundations of neuroscience. *Nat Neurosci* 17(11):1455–1462.

5. Anderson DJ, Perona P (2014) Toward a Science of Computational Ethology. *Neuron* 84(1):18–31.

6. Bishop CM (2006) *Pattern Recognition and Machine Learning* (Springer Verlag).

7. Vogelstein JT, et al. (2014) Discovery of Brainwide Neural-Behavioral Maps via Multiscale Unsupervised Structure Learning. *Science* 344(6182):386–392.

8. Kabra, M., Robie, A. A., Rivera-Alba, M., Branson, S., & Branson, K. (2013). JAABA: Interactive machine learning for automatic annotation of animal behavior. *Nat Meth*, *10*(1), 64–67.

9. Branson K, Robie AA, Bender J, Perona P, Dickinson MH (2009) High-throughput ethomics in large groups of *Drosophila*. *Nat Meth* 6(6):451–457.

10. Dankert H, Wang L, Hoopfer ED, Anderson DJ, Perona P (2009) Automated monitoring and analysis of social behavior in *Drosophila*. *Nat Meth* 6(4):297–303.

11. Baek J-H, Cosman P, Feng Z, Silver J, Schafer WR (2002) Using machine vision to analyze and classify *Caenorhabditis elegans* behavioral phenotypes quantitatively. *J Neurosci Methods* 118(1):9–21.

12. Brown AEX, Yemini EI, Grundy LJ, Jucikas T, Schafer WR (2013) A dictionary of behavioral motifs reveals clusters of genes affecting *Caenorhabditis elegans* locomotion. *Proc Natl Acad Sci USA* 110(2):791–796.

13. Stephens GJ, Johnson-Kerner B, Bialek W, Ryu WS (2008) Dimensionality and Dynamics in the Behavior of *C. elegans*. *PLoS Comput Biol* 4(4):e1000028.

14. Lockery SR (2011) The computational worm: spatial orientation and its neuronal basis in *C. elegans*. *Curr Opin Neurobiol* 21(5):782–790.

15. Suzuki H, et al. (2008) Functional asymmetry in *Caenorhabditis elegans* taste neurons and its computational role in chemotaxis. *Nature* 454(7200):114–117.

16. Chronis N, Zimmer M, Bargmann CI (2007) Microfluidics for in vivo imaging of neuronal and behavioral activity in *Caenorhabditis elegans*. *Nat Meth* 4(9):727–731.

17. Clark DA, Gabel CV, Gabel H, Samuel ADT (2007) Temporal activity patterns in thermosensory neurons of freely moving *Caenorhabditis elegans* encode spatial thermal gradients. *J Neurosci* 27(23):6083–6090.

18. Kimura KD, Miyawaki A, Matsumoto K, Mori I (2004) The *C. elegans* Thermosensory Neuron AFD Responds to Warming. *Curr Biol* 14(14):1291–1295.

19. Tanimoto Y, et al. (2017) Calcium dynamics regulating the timing of decision-making in *C. elegans*. *eLife* 6:13819.

20. Larsch J, Ventimiglia D, Bargmann CI, Albrecht DR (2013) High-throughput imaging of neuronal activity in *Caenorhabditis elegans*. *Proc Natl Acad Sci USA* 110(45):E4266–73.

21. Yemini E, Jucikas T, Grundy LJ, Brown AEX, Schafer WR (2013) A database of *Caenorhabditis elegans* behavioral phenotypes. *Nat Meth* 10(9):877–879.

807 22. Quinlan JR (1986) Induction of Decision Trees. *Mach Learn* 1(1):81–106.

808 23. Brenner S (1974) The genetics of *Caenorhabditis elegans*. *Genetics* 77(1):71–94.

809 24. Kimura KD, Fujita K, Katsura I (2010) Enhancement of odor avoidance
810 regulated by dopamine signaling in *Caenorhabditis elegans*. *J Neurosci*
811 30(48):16365–16375.

812 25. Yamazoe-Umemoto A, Fujita K, Iino Y, Iwasaki Y, Kimura KD (2015)
813 Modulation of different behavioral components by neuropeptide and dopamine
814 signalings in non-associative odor learning of *Caenorhabditis elegans*. *Neurosci*
815 *Res* 99:22–33.

816 26. Pierce-Shimomura JT, Morse TM, Lockery SR (1999) The fundamental role of
817 pirouettes in *Caenorhabditis elegans* chemotaxis. *J Neurosci* 19(21):9557–9569.

818 27. Yamada Y, Hiryu S, Watanabe Y (2016) Species-specific control of acoustic
819 gaze by echolocating bats, Rhinolophus ferrumequinum nippon and Pipistrellus
820 abramus, during flight. *J Comp Physiol A* 202(11):791–801.

821 28. Gorelik R, Gautreau A (2014) Quantitative and unbiased analysis of directional
822 persistence in cell migration. *Nat Protoc* 9(8):1931–1943.

823 29. Iino Y, Yoshida K (2009) Parallel use of two behavioral mechanisms for
824 chemotaxis in *Caenorhabditis elegans*. *J Neurosci* 29(17):5370–5380.

825 30. Quinlan JR (1992) *C4.5* (Morgan Kaufmann, San Mateo).

826 31. Frank E, Hall MA, Witten IH (2016) The WEKA Workbench (Online Appendix).
827 *Data Mining* (Morgan Kaufmann). Forth Edition.

828 32. Tian L, et al. (2009) Imaging neural activity in worms, flies and mice with
829 improved GCaMP calcium indicators. *Nat Meth* 6(12):875–881.

830 33. Shaner NC, et al. (2004) Improved monomeric red, orange and yellow
831 fluorescent proteins derived from *Discosoma sp.* red fluorescent protein. *Nat*
832 *Biotech* 22(12):1567–1572.

833 34. Lewis JA, Wu CH, Berg H, Levine JH (1980) The genetics of levamisole
834 resistance in the nematode *Caenorhabditis elegans*. *Genetics* 95(4):905–928.

835 35. Zheng Y (2015) Trajectory Data Mining. *ACM Trans Intell Syst Technol* 6(3):1–
836 41.

837 36. Louis M, Huber T, Benton R, Sakmar TP, Vosshall LB (2008) Bilateral olfactory
838 sensory input enhances chemotaxis behavior. *Nat Neurosci* 11(2):187–199.

839 37. Kato S, Xu Y, Cho CE, Abbott LF, Bargmann CI (2014) Temporal responses of
840 *C. elegans* chemosensory neurons are preserved in behavioral dynamics. *Neuron*
841 81(3):616–628.

842 38. Teghtsoonian R (1971) On the exponents in Stevens' law and the constant in
843 Ekman's law. *Psycho Rev* 78(1):71–80.

844 39. Kaplan JM (1996) Sensory signaling in *Caenorhabditis elegans*. *Curr Opin*
845 *Neurobiol* 6(4):494–499.

846 40. Bargmann CI (2006) Chemosensation in *C. elegans*. *WormBook*:1–29.

847 41. Kass J, Jacob TC, Kim P, Kaplan JM (2001) The EGL-3 proprotein convertase
848 regulates mechanosensory responses of *Caenorhabditis elegans*. *J Neurosci*
849 21(23):9265–9272.

850 42. Suo S, Ishiura S, Van Tol HHM (2004) Dopamine receptors in *C. elegans*. *Eur J*
851 *Pharmacol* 500(1-3):159–166.

852 43. Tobin D, et al. (2002) Combinatorial expression of TRPV channel proteins
853 defines their sensory functions and subcellular localization in *C. elegans* neurons.
854 *Neuron* 35(2):307–318.

855 44. Colbert HA, Smith TL, Bargmann CI (1997) OSM-9, a novel protein with
856 structural similarity to channels, is required for olfaction, mechanosensation, and
857 olfactory adaptation in *Caenorhabditis elegans*. *J Neurosci* 17(21):8259–8269.

858 45. Komatsu H, Mori I, Rhee JS, Akaike N, Ohshima Y (1996) Mutations in a cyclic
859 nucleotide-gated channel lead to abnormal thermosensation and chemosensation
860 in *C. elegans*. *Neuron* 17(4):707–718.

861 46. Li C, Kim K (2008) Neuropeptides. *WormBook*:1–36.

862 47. Husson SJ, Clynen E, Baggerman G, Janssen T, Schoofs L (2006) Defective
863 processing of neuropeptide precursors in *Caenorhabditis elegans* lacking
864 proprotein convertase 2 (KPC-2/EGL-3): mutant analysis by mass spectrometry.
865 *J Neurochem* 98(6):1999–2012.

866 48. Chase DL, Koelle MR (2007) Biogenic amine neurotransmitters in *C. elegans*.
867 *WormBook*:1–15.

868 49. Moss CF, Surlykke A (2010) Probing the natural scene by echolocation in bats.
869 *Front Behav Neurosci* 4. doi:10.3389/fnbeh.2010.00033.

870 50. Hong W, et al. (2015) Automated measurement of mouse social behaviors using
871 depth sensing, video tracking, and machine learning. *Proc Natl Acad Sci USA*
872 112(38):E5351–E5360.

873 51. Gershow M, et al. (2012) Controlling airborne cues to study small animal
874 navigation. *Nat Meth* 9(3):290–296.

875 52. Albrecht DR, Bargmann CI (2011) High-content behavioral analysis of
876 *Caenorhabditis elegans* in precise spatiotemporal chemical environments. *Nat*
877 *Meth* 8(7):599–605.

878 53. Burges CJC (1998) A tutorial on support vector machines for pattern recognition.
879 *Data Mining and Knowledge Discovery* 2(2):121–167.

880 54. LeCun Y, Bengio Y, Hinton G (2015) Deep learning. *Nature* 521(7553):436–
881 444.

882

883

884 **Table 1. A list of behavioral features used for worms' olfactory navigation**

Parameters	Definition
RunNum	Number of a run
RunTime	Start time of a run
RunDur	Duration of a run
PirDur	Duration of the previous pirouette
V_Ave	Average velocity during a run
V_Ini	Velocity at run initiation
V_Ter	Velocity at run termination
dV_Ave	Average acceleration during a run
dV_Ini	Acceleration at run initiation
dV_Ter	Acceleration at run termination
B_Ave	Bearing of migratory vector throughout a run
B_Ini	Bearing at run initiation
B_Ter	Bearing at run termination
dB_Ave	Average temporal changes in bearing
dB_Ini	Temporal changes in bearing at run initiation
dB_Ter	Temporal changes in bearing at run termination
C_Ave	Average odor concentration during a run
C_Ini	Odor concentration at run initiation
C_Ter	Odor concentration at run termination
dC_Ave	Average temporal changes in odor concentration during a run
dC_Ini	Temporal changes in odor concentration at run initiation
dC_Ter	Temporal changes in odor concentration at run termination
Dir_Ave	Average directionality ratio
Dir_Ini	Directionality ratio at run initiation
Dir_Ter	Directionality ratio at run termination
WV	Curving rate of a run
RunDurΔ	Current *RunDur* minus the previous *RunDur*
PirDurΔ	Current *PirDur* minus the previous *PirDur*
WVΔ	Current *WV* minus the previous *WV*
X_AveΔAve	Current *Ave* minus the previous *Ave*
X_AveΔIni	Current *Ave* minus the previous *Ini*
X_AveΔTer	Current *Ave* minus the previous *Ter*
X_IniΔAve	Current *Ini* minus the previous *Ave*
X_IniΔIni	Current *Ini* minus the previous *Ini*
X_IniΔTer	Current *Ini* minus the previous *Ter*
X_TerΔAve	Current *Ter* minus the previous *Ave*
X_TerΔIni	Current *Ter* minus the previous *Ini*
X_TerΔTer	Current *Ter* minus the previous *Ter*
(*X = V, dV, B, dB, C, dC, Dir*)	

885

886

887 **Table 2. Extracted features of worms' olfactory navigation modulated by prior**
888 **odor experience**

naive vs pre-exp		mock vs pre-exp	
V_Ave	0.1796	***C_Ter***	0.1337
Run_Dur	0.1558	***C_Ave***	0.0998
dB_Ini	0.1349	***C_Ini***	0.0932
C_IniΔAve	0.1230	***dC_Ave***	0.0854
C_IniΔIni	0.1230	*dC_Ini*	0.0810
dB_TerΔIni	0.1191	***dC_Ter***	0.0749
dB_AveΔIni	0.1013	*dC_IniΔTer*	0.0722
C_Ave	0.0983	*dC_TerΔIni*	0.0490
C_Ter	0.0942	*dV_AveΔIni*	0.0478
dB_IniΔTer	0.0924	*dV_Ini*	0.0478
C_Ini	0.0914	*dV_Ave*	0.0364
dB_IniΔAve	0.0839	***Run_Dur***	0.0352
V_AveΔAve	0.0815	***dB_Ini***	0.0342
dC_Ter	0.0810	***dB_TerΔIni***	0.0304
Run_DurΔ	0.0785	***dB_AveΔIni***	0.0298
dC_Ave	0.0547		
C_AveΔTer	0.0394		
Pir_Dur	0.0326		

889 Bold letters indicate features shared between the two comparisons.
890

Table 3. Summary of extracted features of wild-type and mutant strains that are modulated by prior odor experience

strain	*RunDur*	*V_Ave*	*V_Ini*	*V_Ter*	*B_Ter*	*dB_Ini*	*C_Ave*	*C_Ini*	*C_Ter*	*dC_Ave*	*dC_Ter*	*Dir_Ave*	*RunNum*
wild-type	up					down	down	down	down	up	up		
egl-3(n589)							up	up	up				
egl-3(ok979)		down	down	down		down	up	up	up				
dop-3(tm1356)	up	down		down	up					up	up	down	
ocr-2(ak47)		up		up	up								
osm-9(ky10)	up	up		up									
tax-4(p678)													up

Only features with statistical differences between preexposed worms versus naive *and* mock-treated worms are shown.

894 **Table 4. A list of behavioral features used for bats' acoustic navigation**

Parameters	Definition
V(t)	Fight velocity in 3D space
dV(t)	Flight acceleration in 3D space
B_hori(t)	Absolut bearing of the flight vector in a horizontal plane
dB_hori(t)	Temporal change in bearing of the flight vector in a horizontal plane
ddB_hori(t)	Temporal acceleration in bearing of the flight vector in a horizontal plane
B_vert(t)	Absolut bearing of the flight vector in a vertical plane
B_obs(t)	Absolute bearing to the edge point of the nearest chain array
R_obs(t)	Distance from the bat to the edge point of the nearest chain array
R_x(t)	Longitudinal directional distance to the frontal chain array
R_y(t)	Lateral directional distance to the inside pitch of the chain array
dH(t)	Temporal change in flight height

895

896 t = -0.3, -0.2, -0.1, or 0 s. *B_obs(t)* and *R_x(t)* were not calculated for t = 0.

897

898

Figure 1

Behavioral data

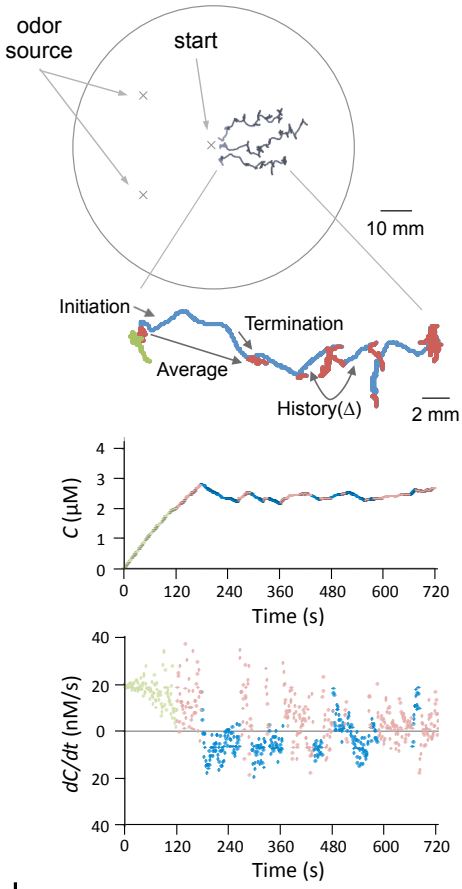

Feature vector

Worm	Run Num	Run Dur	Pir Dur	V			B			C			dV			dB			dC			V_Ave Δ			B_Ave Δ			…
				Ave	Ini	Ter	Ave	Ini	Ter	Ave	Ini	Ter	Ave	Ini	Ter	Ave	Ini	Ter	Ave	Ini	Ter	Ave	Ini	Ter	Ave	Ini	Ter	
1	1																											
1	2																											
1	3																											

Gain ratio

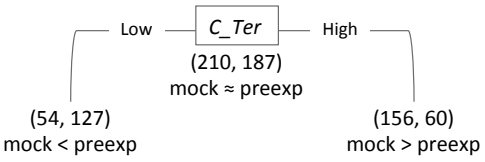

Parameter	mock		preexp		Info	Info gain	Split info	Gain ratio
	Low	High	Low	High				
Original	210		187		0.9976[a]	–	–	–
C_Ter	54	156	127	60	0.8646[b]	0.1329[c] (c = a-b)	0.9944[d]	0.1337[e] (e = c/d)

Figure 2

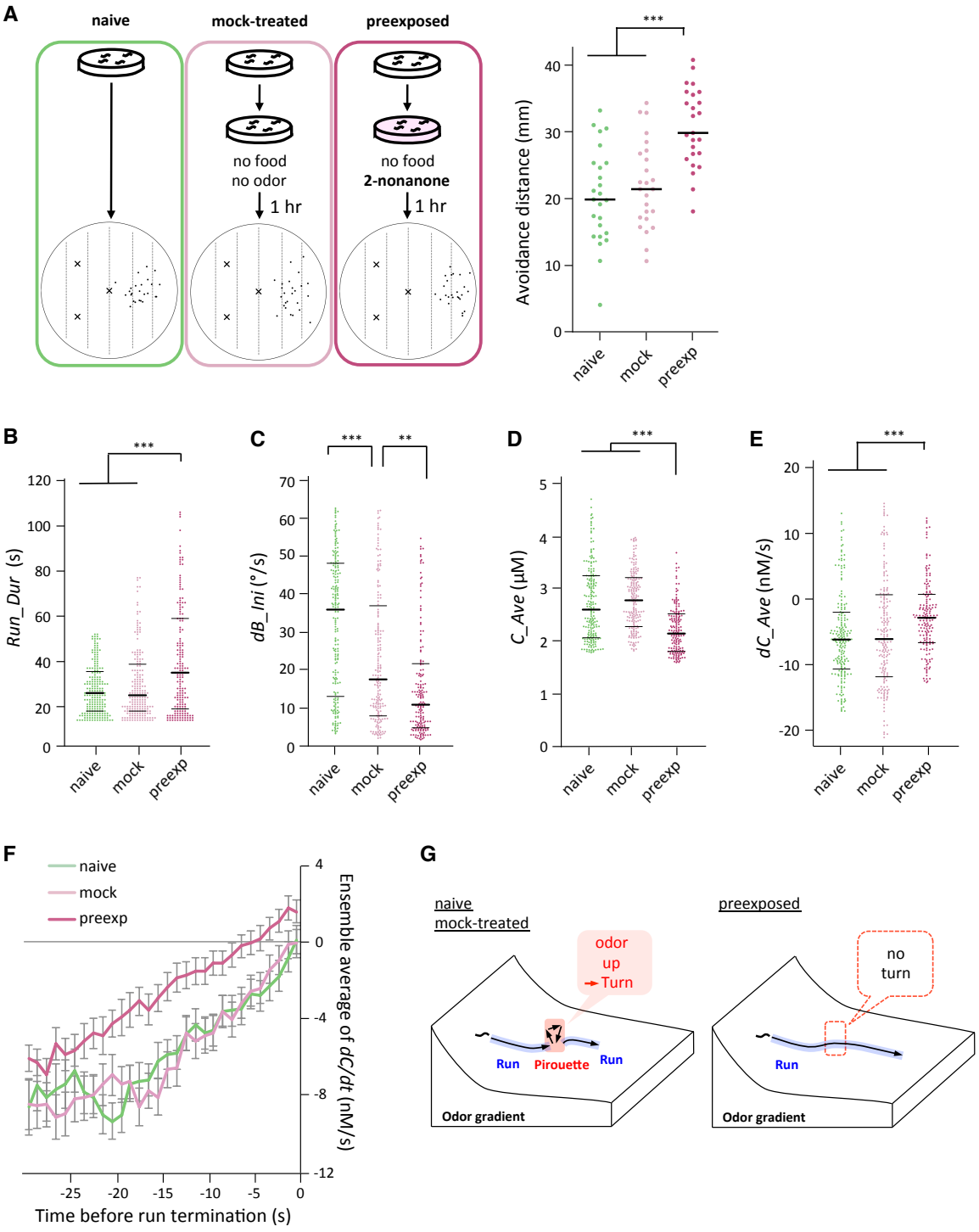
A
naive
mock-treated
preexposed
no food
no odor
1 hr
no food
2-nonanone
1 hr
Avoidance distance (mm)
***
naive
mock
preexp
B
Run_Dur (s)
***
C
dB_Ini (°/s)
***
**
D
C_Ave (µM)
***
E
dC_Ave (nM/s)
***
F
naive
mock
preexp
Ensemble average of dC/dt (nM/s)
Time before run termination (s)
G
naive
mock-treated
odor
up
Turn
Run
Pirouette
Run
Odor gradient
preexposed
no
turn
Run
Odor gradient

Figure 3

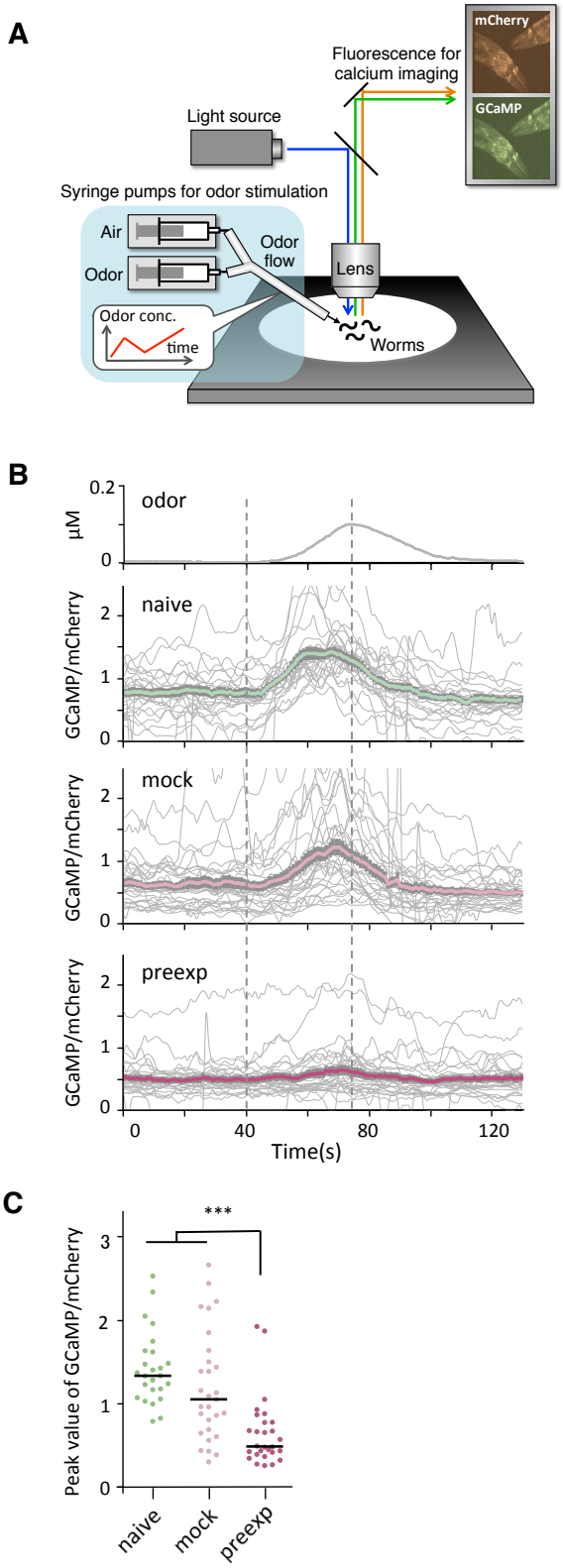
A
Fluorescence for calcium imaging
mCherry
GCaMP
Light source
Syringe pumps for odor stimulation
Air
Odor
Odor flow
Lens
Odor conc.
time
Worms
B
odor
μM
0.2
0
naive
mock
preexp
GCaMP/mCherry
2
1
0
0
40
80
120
Time(s)
C
***
Peak value of GCaMP/mCherry
3
2
1
0
naive
mock
preexp

Figure 4

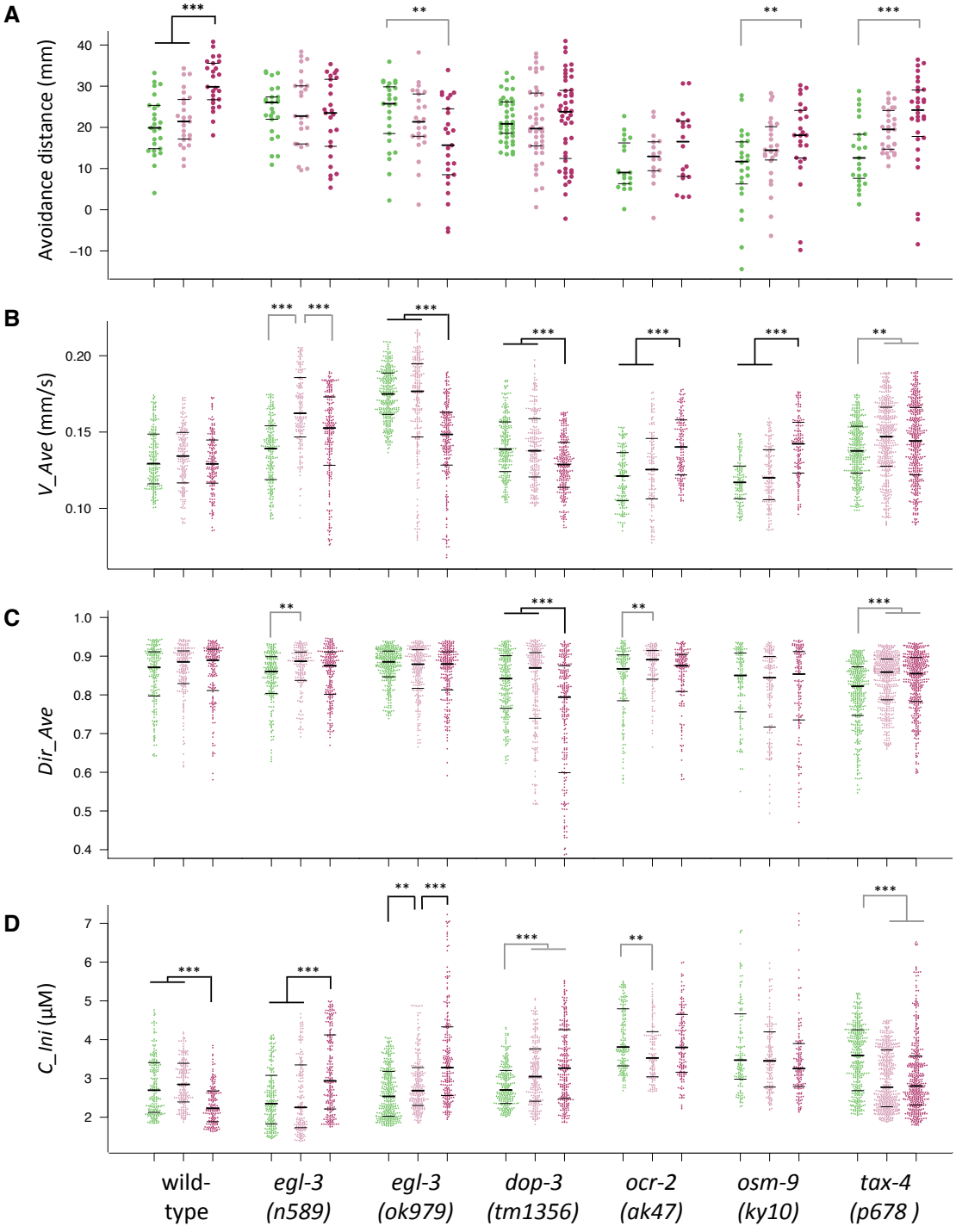
A
Avoidance distance (mm)
B
V_Ave (mm/s)
C
Dir_Ave
D
C_Ini (µM)
wild-type
egl-3 (n589)
egl-3 (ok979)
dop-3 (tm1356)
ocr-2 (ak47)
osm-9 (ky10)
tax-4 (p678)

Figure 5

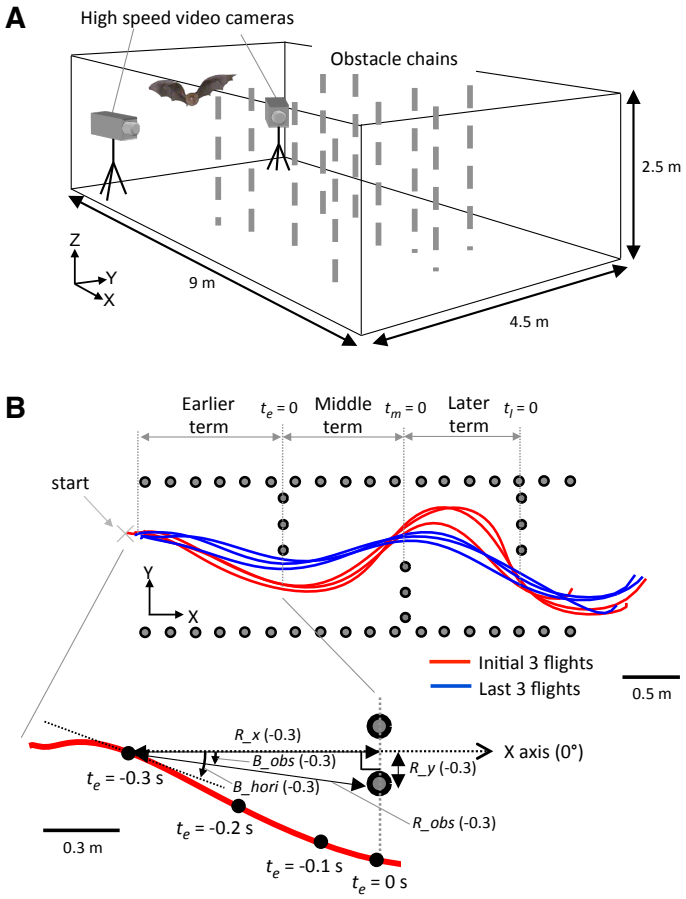

C

Features	Gain ratio
R_x (-0.3)	0.373
R_obs (-0.3)	0.352
V (-0.3)	0.312
V (-0.2)	0.294
R_x (-0.2)	0.294
R_obs (-0.2)	0.294
B_hori (-0.3)	0.292
B_hori (-0.2)	0.219
ddB_hori (-0.3)	0.209

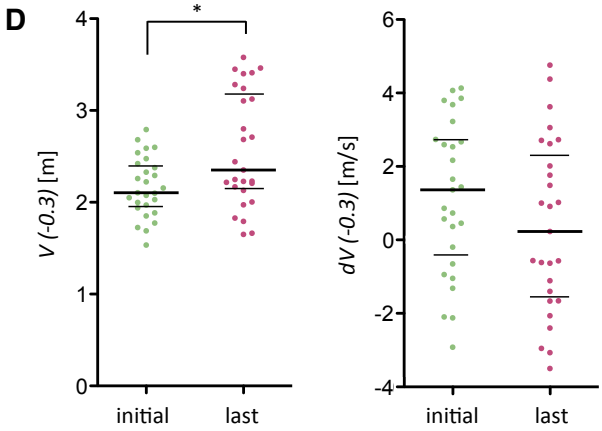

Supplementary Table 1

Supplementary Table 1. Detailed results of statistical tests.

Figure	Parameter	Number of naive	Number of mock	Number of preexp.	Unit of number	Multiple test	df value of multiple test	p value of multiple test	Other result of multiple test	Post-hock test	df value of post-hock test	p value of post-hock test	Other result of post-hock test
2A, 4A	Avoidance distance of N2	25	25	25	animals	Kruskal-Wallis test	2	<0.0001(***)	24.451	Dunn's test	1	naive vs mock: 0.7621(ns) naive vs preexposure: <0.0001(***) mock vs preexposure: 0.0001(***)	z = 0.6619 z = 4.5747 z = 3.9128
2B	Run duration of N2	219	210	187	runs	Kruskal-Wallis test	2	<0.0001(***)	18.76	Dunn's test	1	naive vs mock: 1(ns) naive vs preexposure: <0.0001(***) mock vs preexposure: 0.0006(***)	z = -0.4269 z = -3.9959 z = -3.547
2C	Initial dBearing of N2	219	210	187	runs	Mardia-Watson-Wheeler test	2	<0.0001(***)	64.69	Mardia-Watson-Wheeler test	1	naive vs mock: <0.0001(***) naive vs preexposure: <0.0001(***) mock vs preexposure: 0.002(**)	W = 26.305 W = 59.795 W = 12.007
2D	Average Conc. of N2	219	210	187	runs	Kruskal-Wallis test	2	<0.0001(***)	68.69	Dunn's test	1	naive vs mock: 0.1351(ns) naive vs preexposure: <0.0001(***) mock vs preexposure: <0.0001(***)	z = -1.6951 z = 6.3349 z = 7.9016
2E	Averege dConc. of N2	219	210	187	runs	Kruskal-Wallis test	2	0.0003(***)	16.56	Dunn's test	1	naive vs mock: 0.3202(ns) naive vs preexposure: <0.0001(***) mock vs preexposure: 0.0085(**)	z = -1.2441 z = -4.001 z = -2.7671
3C	Peak value of GCaMP3/mCherry	25	29	28	animals	Kruskal-Wallis test	2	<0.0001(***)	30.11	Dunn's test	1	naive vs mock: 0.0949(ns) naive vs preexposure: <0.0001(***) mock vs preexposure: 0.0004(***)	z = 1.8571 z = 5.3589 z = 3.6525
4A	Avoidance distance of *egl-3(n589)*	25	25	25	animals	Kruskal-Wallis test	2	0.7763(ns)	0.51	Dunn's test	1	-	-
4A	Avoidance distance of *egl-3(ok979)*	25	25	25	animals	Kruskal-Wallis test	2	0.0128(*)	8.72	Dunn's test	1	naive vs mock: 0.3924(ns) naive vs preexposure: 0.0051(**) mock vs preexposure: 0.1069(ns)	z = -1.1226 z = -2.9265 z = -1.8039
4A	Avoidance distance of *dop-3(tm1356)*	46	46	47	animals	Kruskal-Wallis test	2	0.8196(ns)	0.40	Dunn's test	1	-	-
4A	Avoidance distance of *ocr-2(ak47)*	19	16	18	animals	Kruskal-Wallis test	2	0.2001(ns)	3.22	Dunn's test	1	-	-
4A	Avoidance distance of *osm-9(ky10)*	24	26	24	animals	Kruskal-Wallis test	2	0.0191(*)	7.91	Dunn's test	1	naive vs mock: 0.1625(ns) naive vs preexposure: 0.0075(**) mock vs preexposure: 0.3141(ns)	z = 1.6058 z = 2.8055 z = 1.2552
4A	Avoidance distance of *tax-4(p678)*	23	29	30	animals	Kruskal-Wallis test	2	0.0008(***)	14.39	Dunn's test	1	naive vs mock: 0.0506(ns) naive vs preexposure: 0.0002(***) mock vs preexposure: 0.1175(ns)	z = 2.1232 z = 3.7932 z = 1.7605
4B	Average speed of N2	219	210	187	runs	Kruskal-Wallis test	2	0.2796(ns)	2.55	Dunn's test	1	-	-
4B	Average speed of *egl-3(n589)*	227	194	235	runs	Kruskal-Wallis test	2	<0.0001(***)	80.44	Dunn's test	1	naive vs mock: <0.0001(***) naive vs preexposure: <0.0001(***) mock vs preexposure: <0.0001(***)	z = -8.9653 z = -4.5544 z = 4.6671
4B	Average speed of *egl-3(ok979)*	370	260	252	runs	Kruskal-Wallis test	2	<0.0001(***)	137.51	Dunn's test	1	naive vs mock: 0.3296(ns) naive vs preexposure: <0.0001(***) mock vs preexposure: <0.0001(***)	z = 1.2272 z = 11.1444 z = 9.1734
4B	Average speed of *dop-3(tm1356)*	276	266	279	runs	Kruskal-Wallis test	2	<0.0001(***)	39.19	Dunn's test	1	naive vs mock: 0.6155(ns) naive vs preexposure: <0.0001(***) mock vs preexposure: <0.0001(***)	z = 0.8234 z = 5.795 z = 4.9154
4B	Average speed of *ocr-2(ak47)*	180	142	168	runs	Kruskal-Wallis test	2	<0.0001(***)	50.52	Dunn's test	1	naive vs mock: 0.075(ns) naive vs preexposure: <0.0001(***) mock vs preexposure: <0.0001(***)	z = -1.9599 z = -6.9657 z = -4.6254
4B	Average speed of *osm-9(ky10)*	147	175	160	runs	Kruskal-Wallis test	2	<0.0001(***)	66.85	Dunn's test	1	naive vs mock: 0.2053(ns) naive vs preexposure: <0.0001(***) mock vs preexposure: <0.0001(***)	z = -1.4875 z = -7.5979 z = -6.4146
4B	Average speed of *tax-4(p678)*	402	531	473	runs	Kruskal-Wallis test	2	<0.0001(***)	20.69	Dunn's test	1	naive vs mock: <0.0001(***) naive vs preexposure: 0.0019(**) mock vs preexposure: 0.3492(ns)	z = -4.456 z = -3.2307 z = 1.1931
4C	Average directionality ratio of N2	219	210	187	runs	Kruskal-Wallis test	2	0.2781(ns)	2.56	Dunn's test	1	-	-
4C	Average directionality ratio of *egl-3(n589)*	227	194	235	runs	Kruskal-Wallis test	2	0.0042(**)	10.96	Dunn's test	1	naive vs mock: 0.0014(**) naive vs preexposure: 0.1115(ns) mock vs preexposure: 0.1585(ns)	z = -3.3036 z = -1.7844 z = 1.6179
4C	Average directionality ratio of *egl-3(ok979)*	370	260	252	runs	Kruskal-Wallis test	2	0.1357(ns)	4.00	Dunn's test	1	-	-
4C	Average directionality ratio of *dop-3(tm1356)*	276	266	279	runs	Kruskal-Wallis test	2	<0.0001(***)	38.61	Dunn's test	1	naive vs mock: 1(ns) naive vs preexposure: <0.0001(***) mock vs preexposure: <0.0001(***)	z = -0.3986 z = 5.1836 z = 5.5349
4C	Average directionality ratio of *ocr-2(ak47)*	180	142	168	runs	Kruskal-Wallis test	2	0.0135(*)	8.62	Dunn's test	1	naive vs mock: 0.0062(**) naive vs preexposure: 0.6577(ns) mock vs preexposure: 0.0541(ns)	z = -2.8694 z = -0.7747 z = 2.0962
4C	Average directionality ratio of *osm-9(ky10)*	147	175	160	runs	Kruskal-Wallis test	2	0.6949(ns)	0.73	Dunn's test	1	-	-
4C	Average directionality ratio of *tax-4(p678)*	402	531	473	runs	Kruskal-Wallis test	2	<0.0001(***)	37.08	Dunn's test	1	naive vs mock: <0.0001(***) naive vs preexposure: <0.0001(***) mock vs preexposure: 1(ns)	z = -5.4554 z = -5.2773 z = 0.0423
4D	Initial Conc. of N2	219	210	187	runs	Kruskal-Wallis test	2	<0.0001(***)	57.75	Dunn's test	1	naive vs mock: 0.1381(ns) naive vs preexposure: <0.0001(***) mock vs preexposure: <0.0001(***)	z = -1.6846 z = 5.7215 z = 7.284
4D	Initial Conc. of *egl-3(n589)*	227	194	235	runs	Kruskal-Wallis test	2	<0.0001(***)	48.82	Dunn's test	1	naive vs mock: 1(ns) naive vs preexposure: <0.0001(***) mock vs preexposure: <0.0001(***)	z = 0.0374 z = -6.0955 z = -5.8855
4D	Initial Conc. of *egl-3(ok979)*	370	260	252	runs	Kruskal-Wallis test	2	<0.0001(***)	83.00	Dunn's test	1	naive vs mock: 0.002(**) naive vs preexposure: <0.0001(***) mock vs preexposure: <0.0001(***)	z = -3.2048 z = -9.0932 z = -5.4678
4D	Initial Conc. of *dop-3(tm1356)*	276	266	279	runs	Kruskal-Wallis test	2	<0.0001(***)	30.83	Dunn's test	1	naive vs mock: 0.001(***) naive vs preexposure: <0.0001(***) mock vs preexposure: 0.064(ns)	z = -3.4101 z = -5.4972 z = -2.0269
4D	Initial Conc. of *ocr-2(ak47)*	180	142	168	runs	Kruskal-Wallis test	2	0.0151(*)	8.38	Dunn's test	1	naive vs mock: 0.0057(**) naive vs preexposure: 0.2973(ns) mock vs preexposure: 0.1517(ns)	z = 2.8947 z = 1.2868 z = -1.6393
4D	Initial Conc. of *osm-9(ky10)*	147	175	160	runs	Kruskal-Wallis test	2	0.0637(ns)	5.51	Dunn's test	1	-	-
4D	Initial Conc. of *tax-4(p678)*	402	531	473	runs	Kruskal-Wallis test	2	<0.0001(***)	76.84	Dunn's test	1	naive vs mock: <0.0001(***) naive vs preexposure: <0.0001(***) mock vs preexposure: 0.8193(ns)	z = 8.0792 z = 7.3115 z = -0.6035

Figure	Parameter	Number of Groups	Number of initial	Number of last	Unit of number	Statistical tests used	p value	Other result
5D	Fight velocity in 3D space at t=−0.3	2	27	27	flights	Mann–Whitney test	0.0234(*)	Mann-Whitney U = 233.0
5D	Flight acceleration in 3D space at t=−0.3	2	27	27	flights	Mann–Whitney test	0.2326(ns)	Mann-Whitney U = 295.0